

FULL PAPER

Open Access



# Effects of random 3D upper crustal heterogeneity on long-period ( $\geq 1$ s) ground-motion simulations

Asako Iwaki<sup>\*</sup> , Takahiro Maeda, Nobuyuki Morikawa, Shunsuke Takemura and Hiroyuki Fujiwara

## Abstract

The effects of the short-wavelength heterogeneity of the crustal structure on predicted ground motion at periods of 1 s and longer were investigated by conducting three-dimensional finite-difference simulations using a detailed realistic velocity model of the Kanto region of Japan. The short-wavelength heterogeneity of the media within the upper crust was randomly modeled using the exponential-type autocorrelation function where the velocity standard deviation was set to 5%. Combinations of heterogeneous media with various correlation lengths and point source models with various depths and durations were considered in order to investigate the variability of the predicted ground motion and the sensitivity to the parameters. The effects of random heterogeneity on the simulated ground motion appeared as a result of changes in the amplitude and phase of both the direct waves and later phases, as well as the spectral peaks of the response spectra. Ground-motion variability, in terms of peak ground velocity (PGV) and velocity response spectra (Sv), was evaluated using the residual, or the difference in logarithm of PGV and Sv between the ground motion computed with and without random heterogeneity. While the residual averaged over the surface of the computed area was almost negligible in the studied period range, the variability of the residual was found to increase with distance and to be larger for point sources with shorter durations.

**Keywords:** Long-period ground motion, Ground-motion variability, Seismic wave propagation, Crustal heterogeneity, Kanto Plain

## Introduction

In ground-motion simulations for the purpose of seismic hazard evaluation, long-period components (periods of approximately 1 s and longer) are generally evaluated by deterministic numerical simulations using rupture and wave propagation models. The lower limit of the period range for the deterministic simulation is restricted by the difficulty in detailed modeling of the rupture and wave propagation processes in the short-period ( $< 1$  s) range in which the behavior of the seismic waves becomes less coherent.

In order to overcome this limitation, kinematic source parameters in deterministic simulations are often modeled by a combination of deterministic and stochastic

description (e.g., Hisada 2001; Sekiguchi et al. 2008; Graves and Pitarka 2016; Wirth et al. 2017). Iwaki et al. (2016) showed that introducing small-scale heterogeneity to source parameters tends to amplify the simulated long-period ground motion ( $\geq 2$  s), which therefore matches the observed ground motion more satisfactorily. This analysis was on the assumption that the velocity model is appropriate, which is not thoroughly verified.

Development of detailed three-dimensional (3D) seismic velocity models for ground-motion simulations has been carried out, for example, in Japan (e.g., Fujiwara et al. 2009; Koketsu et al. 2012) and in the USA (e.g., Magistrale et al. 2000; Shaw et al. 2015) in order to achieve more reliable simulations. Still, the velocity models are generally much simpler than the realistic Earth structure, which contains heterogeneity on various scales. Japanese 3D velocity models are usually composed of a number of layers, within which the seismic velocity

<sup>\*</sup>Correspondence: iwaki@bosai.go.jp  
National Research Institute for Earth Science and Disaster Resilience, 3-1  
Tennodai, Tsukuba, Ibaraki 305-0006, Japan

is uniform (e.g., Koketsu et al. 2012). Since more accuracy, at least down to period of 1 s, is required in ground-motion simulations, it is important to evaluate the effects of short-wavelength heterogeneity in the media.

Short-wavelength (several kilometers or less) heterogeneity of the media is generally represented by a statistical description of the random perturbation of the elastic properties, which is referred to hereinafter as random heterogeneity. Studies on short-period (generally < 1 s) seismic wave propagation within random media have been developed based on seismic wave propagation and scattering theory (e.g., Sato et al. 2012). The effects of the random heterogeneity on the amplitudes and phases of seismic waves have been revealed by numerical simulations of wave propagation, often focusing on periods shorter than 1 s (e.g., Frankel and Clayton 1984; Imperatori and Mai 2013; Takemura et al. 2015, 2017). However, random crustal heterogeneity also affects ground motion at periods longer than 1 s (e.g., Emoto et al. 2017), which is important from a seismic hazard point of view, because random crustal heterogeneity significantly increases ground-motion variability (e.g., Hartzell et al. 2010).

In the present study, we conduct 3D finite-difference ground-motion simulations using a detailed velocity model of the Kanto region of Japan in order to evaluate the effects of random crustal heterogeneity on the predicted ground motion on the engineering bedrock, in an attempt to improve seismic hazard evaluation by a deterministic approach in the long-period range (> 1 s). Although the precise values of the parameters to model the realistic local crustal heterogeneity have not been sufficiently resolved yet (e.g., Gaebler et al. 2015), we consider several values of parameters to investigate their effects, focusing on, in particular, (1) the ground-motion variability caused by the random media and (2) the sensitivity of the ground motion to the media and source parameters.

## Simulation models

### Kanto velocity model

We use a detailed 3D seismic velocity model of the Kanto region that is used in the National Seismic Hazard Map of Japan by the Headquarters for Earthquake Research Promotion (HERP; HERP 2017). This model covers the subsurface structure from the engineering bedrock ( $V_S \sim 350$ – $700$  m/s) to the seismic bedrock ( $V_S \sim 3200$  m/s) and was constructed in order to improve ground-motion evaluation especially at periods of 0.5–2 s in Kanto (e.g., Senna et al. 2013) compared to the conventionally used J-SHIS version 2 model (Fujiiwara et al. 2009; <http://www.j-shis.bosai.go.jp>). The minimum S-wave velocity in the sedimentary layers of the Kanto Plain is 350 m/s. Below the seismic bedrock, the

subsurface structure model is combined with the crustal model of the Japan Integrated Velocity Structure Model (JIVSM; Koketsu et al. 2012) down to a depth of 70 km. Figure 1 shows maps of the study area, showing the upper boundaries of the selected layers ( $V_S = 700$ , 1500, and 3200 m/s) of the velocity model. Since we focus on the ground motion on the engineering bedrock, the shallow subsurface and topography is not included in this velocity model. Thus, seismic scattering due to topographic variation is not considered in this study. We consider topographic effects to be less influential because the study area is dominated by the Kanto Plain.

### Random 3D heterogeneity

We model the heterogeneity in the upper crust ( $V_S = 3200$ – $3400$  m/s) randomly by introducing the fluctuation of the seismic velocity:

$$V(\mathbf{r}) = V_0(1 + d(\mathbf{r})), \quad (1)$$

where  $V(\mathbf{r})$  is the seismic velocity (for both  $V_S$  and  $V_P$ ) at  $\mathbf{r}$  and  $V_0$  is the background velocity. The assumed fluctuation  $d(\mathbf{r})$  is characterized by the exponential autocorrelation function (e.g., Sato et al. 2012)

$$R(r) = \varepsilon^2 \exp(-r/a), \quad (2)$$

where  $\varepsilon$  and  $a$  are the standard deviation and correlation length, respectively, and the power spectrum for 3D case is

$$P(\mathbf{k}) = \frac{8\pi\varepsilon^2 a^2}{(1 + a^2 \mathbf{k}^2)^2}. \quad (3)$$

The exponential autocorrelation function corresponds to the von Kármán autocorrelation function with decay order of  $\kappa = 0.5$ , which controls the decay rate of the power spectrum at large wavenumbers. Random heterogeneity is generated in the wavenumber ( $\mathbf{k}$ ) domain by adjusting the designed power spectra [Eq. (3)] to a 3D Fourier transformation of a sequence of random numbers. Thus, different random seeds yield different random heterogeneity models.

We modeled the fluctuation with  $\varepsilon = 0.05$  and  $a = 1, 3$ , and 5 km, assuming the correlation lengths in the horizontal and vertical components are identical. These values are consistent with those proposed in previous studies (summarized in Fig. 12 of Emoto et al. 2017). The maximum and minimum seismic velocities with fluctuation are set to mean  $\pm 3\varepsilon$ . Hereinafter, the velocity models with and without random heterogeneity in the upper crust are referred to as the heterogeneous and homogeneous velocity models, respectively. The random heterogeneity in the upper crust (shallower than approximately

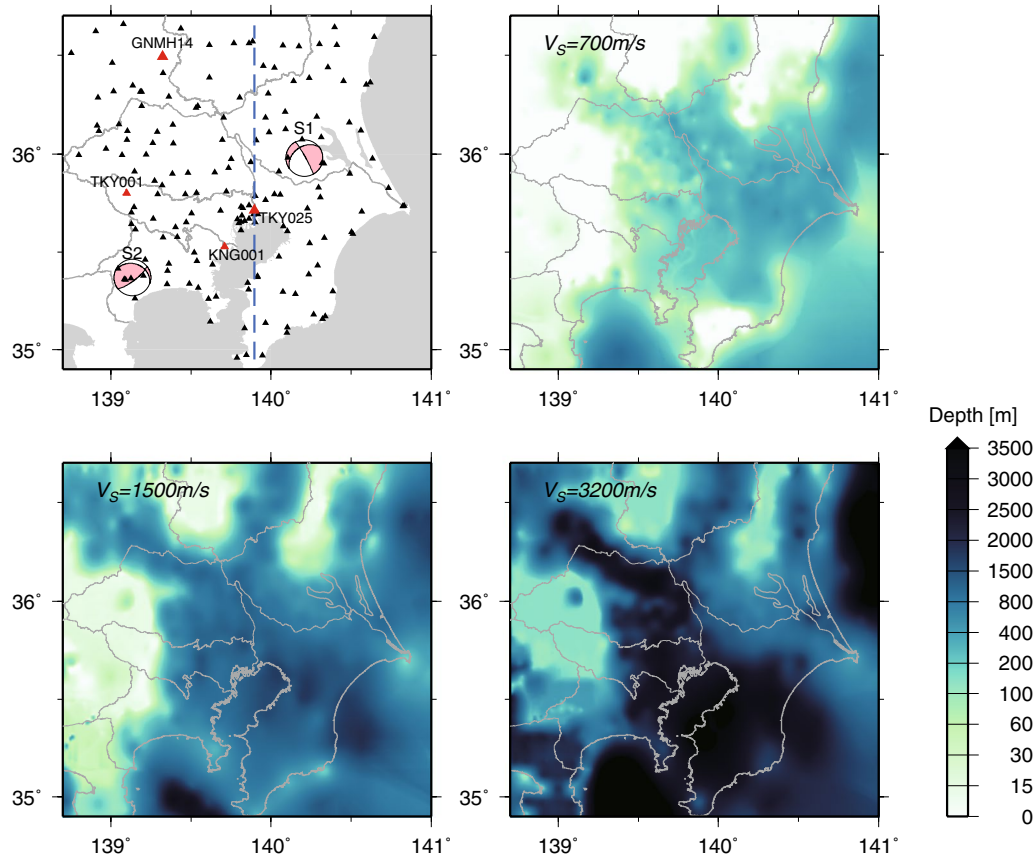


**Fig. 1** Maps of the study area. K-NET and KiK-net stations (triangles) and epicenters of the source models S1 and S2 (top left panel). Dashed line denotes the north–south cross section of Fig. 2. Map of the velocity model showing the upper boundaries of selected layers (top right and bottom panels)

50 km) is considered to be more influential with respect to seismic waves than the deeper parts of the Earth (e.g., Gusev and Abubakirov 1999; Takemura et al. 2017). In the Kanto Plain, a vast area of the upper crust is covered by thick (up to several kilometers) sedimentary layers (see Fig. 1). North–south cross-sectional view of the S-wave velocity for the homogeneous and heterogeneous velocity models is shown in Fig. 2.

In this study, heterogeneity is considered only in the upper crust for the sake of computational efficiency in constructing the velocity models for the simulations. The thickness of the upper crust is approximately 10 km in the target region (see Fig. 2). The effect of heterogeneity in the lower crust was tested by 3D finite-difference simulations using a simpler model. Introducing heterogeneity in the lower crust in addition to the upper crust results in only slight differences in the ground motion, as shown in Additional file 1.

Scattering effects are expected to appear in seismic waves with wavelengths generally equal to or shorter than the correlation length of the random media (e.g.,

Sato et al. 2012). In this case, waves with wave lengths of 1, 3, and 5 km have periods of approximately 0.3, 0.9, and 1.5 s, respectively, in the media with  $V_s = 3200$  m/s. Minimum mean free paths are 55, 17, and 10 km for  $a = 1, 3$ , and 5 km, respectively, with  $\varepsilon = 0.05$ , which is roughly consistent with the variety of the estimated values of scattering coefficient for the lithosphere (Fig. 1.3 of Sato et al. 2012). Therefore, the systematic influence of seismic scattering may be limited in the period range in the present study (1 s and longer). However, it is important to evaluate the effects of random crustal heterogeneity on the predicted ground motion in a realistic areal range, at least  $200\text{--}300\text{ km}^2$ , for seismic hazard assessment in the Kanto region.

#### Ground-motion simulation

We use point source models as virtual seismic sources, located in the center of the Kanto Plain at a depth of 40 km and in the west of the Kanto Plain at a depth of 8 km, referred to as S1 and S2, respectively (see Fig. 1 for the locations of the source models). S1 and S2 are

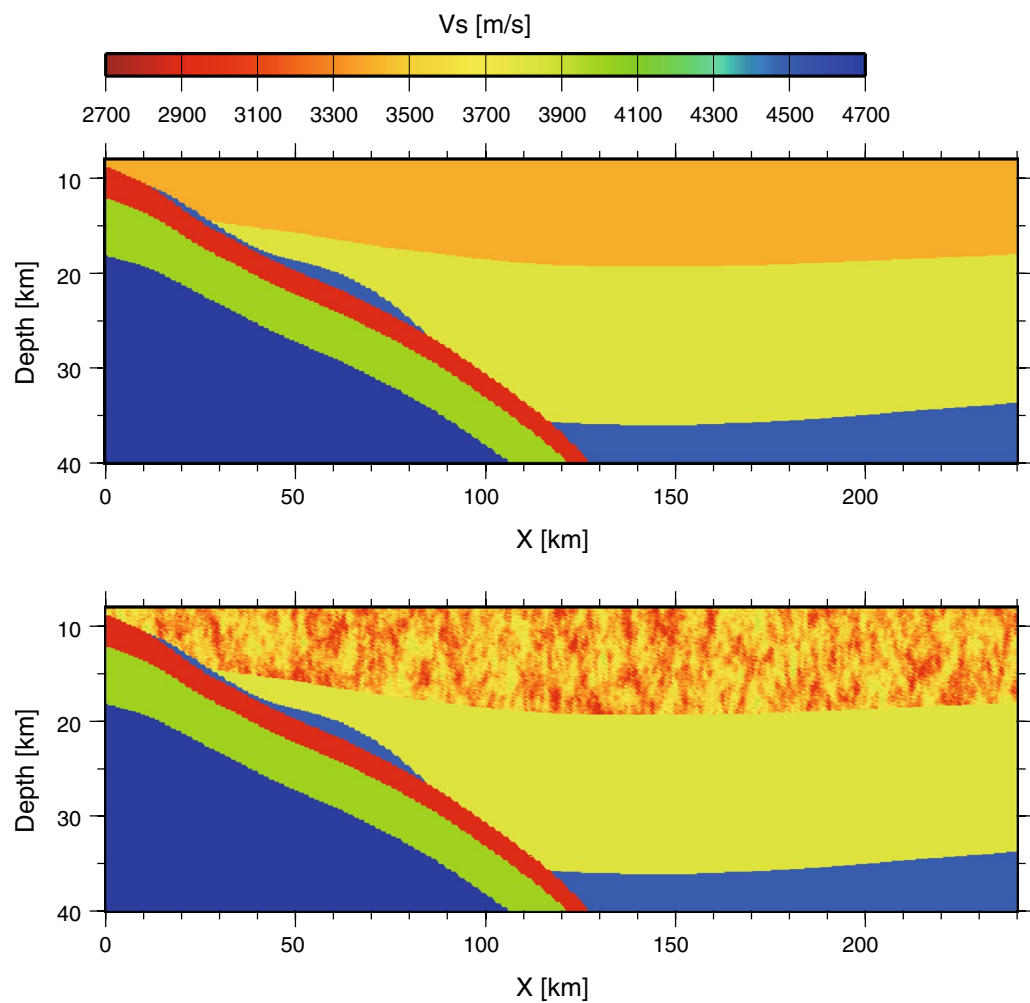


**Fig. 2** North–south cross-sectional view of the S-wave velocity for the homogeneous (top) and heterogeneous (bottom) velocity models. See Fig. 1 for the location of the cross section

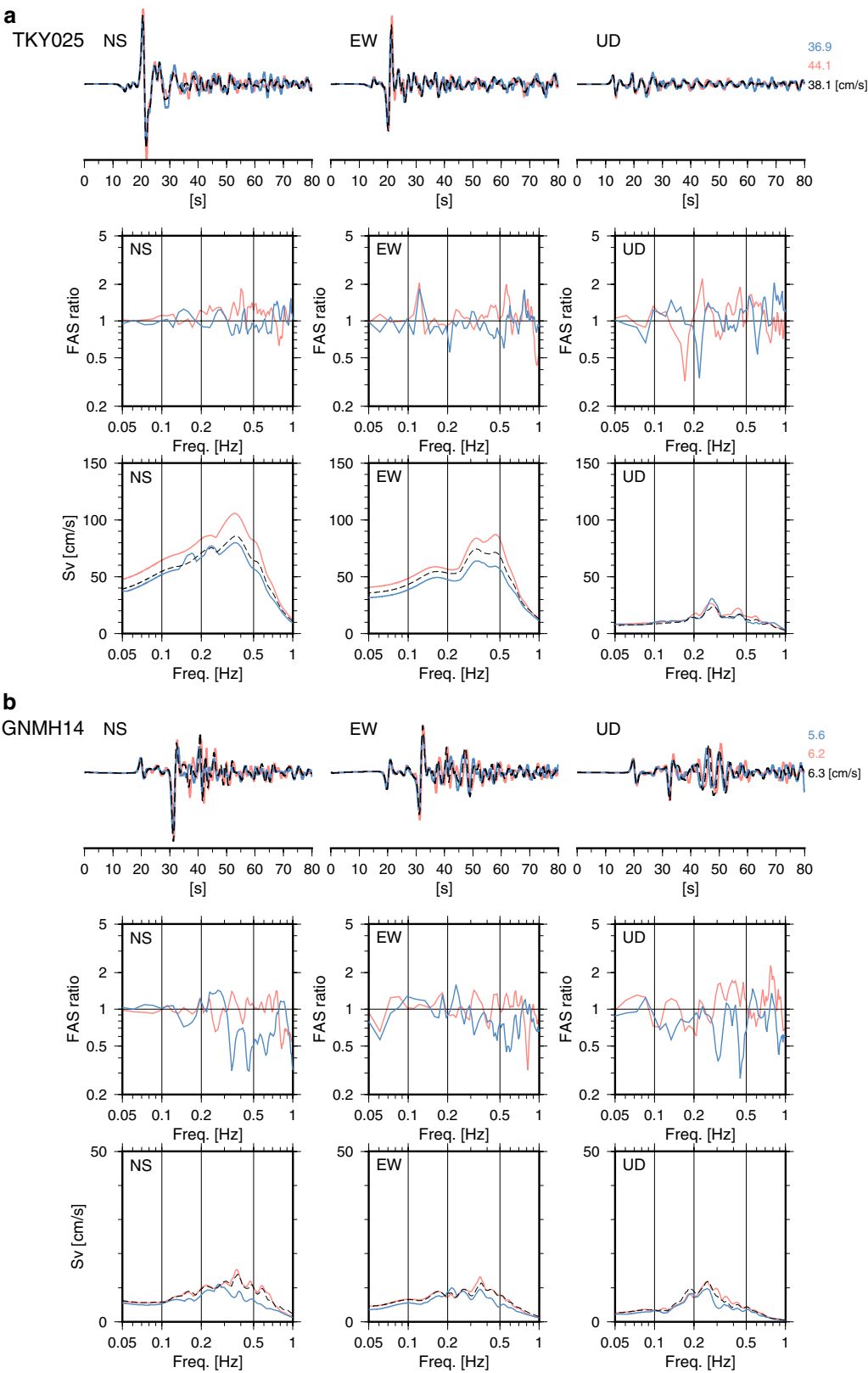
**Table 1** Point source models

	Location <sup>a</sup>	Depth (km)	Duration (s)	Strike, dip, rake (°)
S1_3.3	S1	40	3.3	234, 39, −9
S1_0.5	S1	40	0.5	234, 49, −9
S2_3.3	S2	8	3.3	290, 25, 145

<sup>a</sup> See Fig. 1 for the location of S1 and S2

located near the subducting Philippine Sea Plate, but S1 is within the Oceanic mantle, whereas S2 is in the upper crust where the random heterogeneity is introduced. The source time function is expressed by differentiated smoothed ramp functions with rise times of 3.3 and 0.5 s. Three source models are used in this study as listed in Table 1. The focal mechanism of S1 is taken from a  $M_w$

(See figure on next page.)  
**Fig. 3** Simulated ground motion at selected stations. Velocity waveforms, Fourier amplitude spectral ratios (ratios of heterogeneous to homogeneous models), and 5% damped velocity response spectra for the source model S1\_3.3 using the homogeneous (black dashed lines) and heterogeneous (blue and red lines; representing two realizations with different random seeds) velocity models with  $a=5$  km at **a** TKY025 and **b** GNMH14. Numbers on the right side of the waveforms denote the maximum amplitudes of three components. See Fig. 1 for the location of the stations



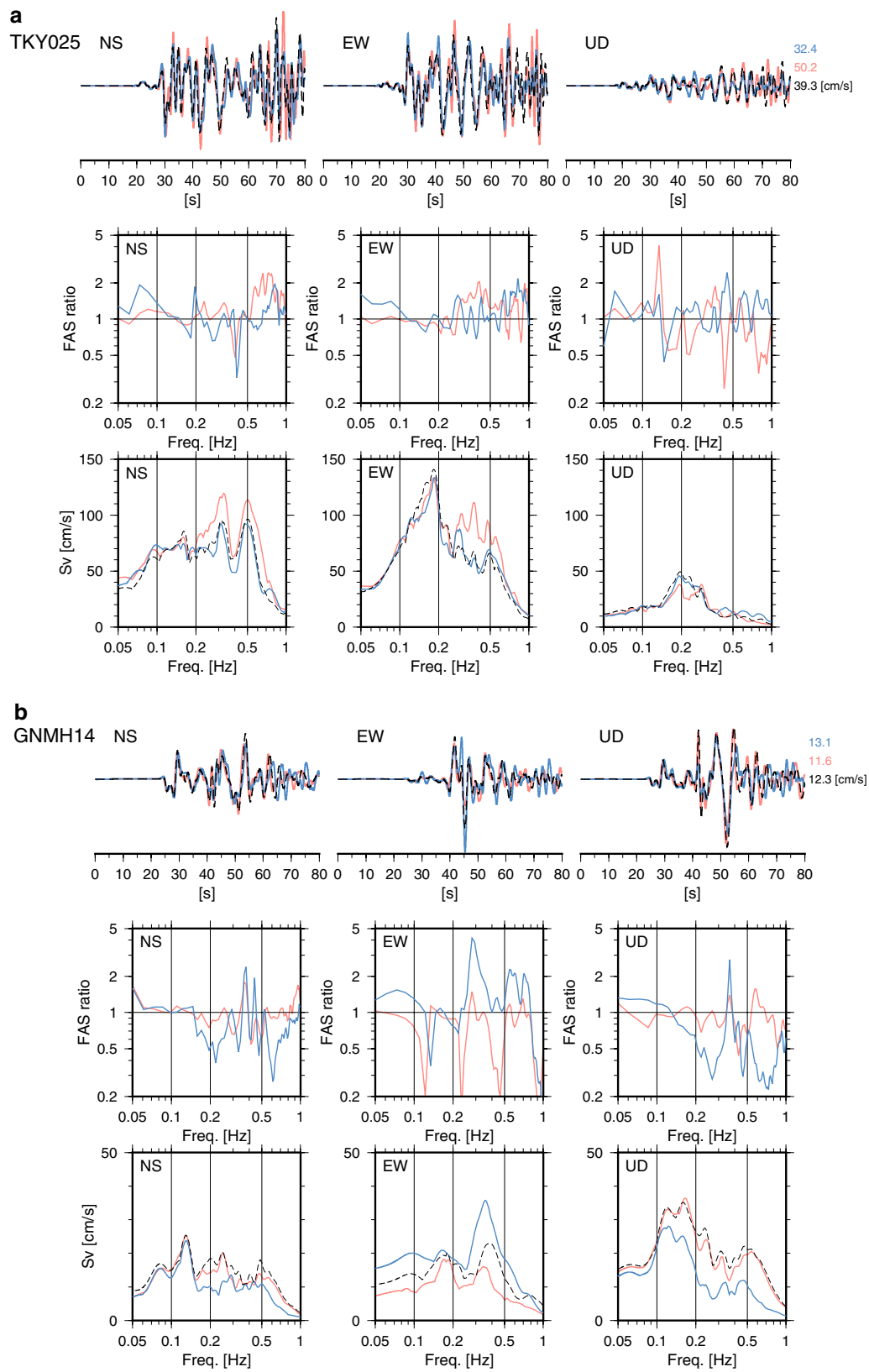


**Fig. 4** Simulated ground motion at selected stations. Same as Fig. 3 but for the source model S2\_3.3



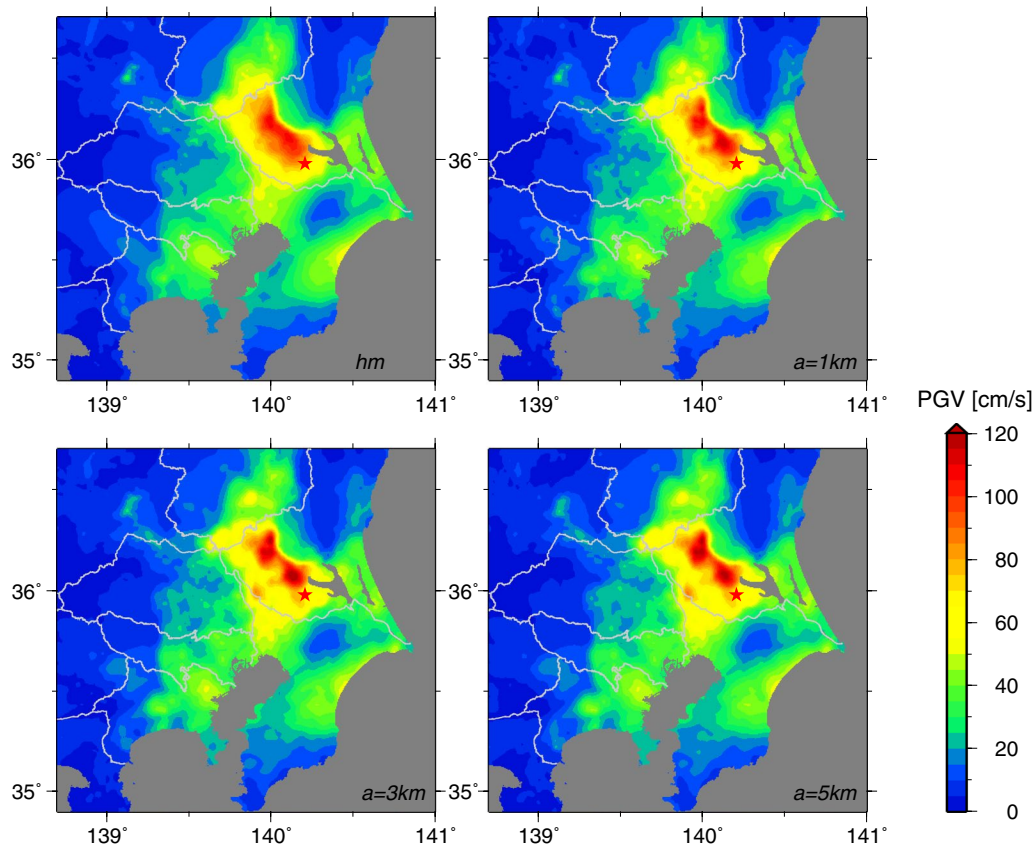


**Fig. 5** Simulated peak ground velocity (PGV) of the simulated ground motion. Comparison of PGV for the homogeneous (upper left panel) and the heterogeneous models with  $a = 1, 3, 5$  km (upper right, bottom left, and bottom right panels, respectively). Red star denotes the epicenter of the source model S1\_3.3

4.7 local event on January 30, 2015, 11:31 (UT) estimated by F-net (Okada et al. 2004; <http://www.fnet.bosai.go.jp/top.php?LANG=en>). For S2, we used the strike and dip angles of the fault model of the 1923 Kanto earthquake ( $M_S$  8.2) (e.g., Sato et al. 1998). Moment magnitudes for all source models are adjusted to 7.0.

We compute the ground-motion time histories on the engineering bedrock with a minimum S-wave velocity of 350 m/s. Ground-motion simulations are conducted by a 3D finite-difference method with discontinuous grids (Aoi and Fujiwara 1999) using an open-source software GMS (Aoi et al. 2004). The maximum frequency of the target is 1 Hz. The computation covers the Kanto region as shown in Fig. 1, approximately 290 km (north–south)

by 260 km (east–west). The grid spacing of the finite-difference simulations is set to 70 m and 35 m in the horizontal and vertical directions, respectively, in the region shallower than 8 km. The grid spacing is three times larger in the deeper region, which yields approximately 5 billion grid points in total. The simulated ground motion is low-pass filtered at 1 Hz.

Anelastic attenuation is modeled by multiplying the updates in velocity and stress fields at each time step by

$$A(x, y, z) = \exp \left[ \frac{-\pi f_0 \Delta t}{Q(x, y, z)} \right], \quad (4)$$

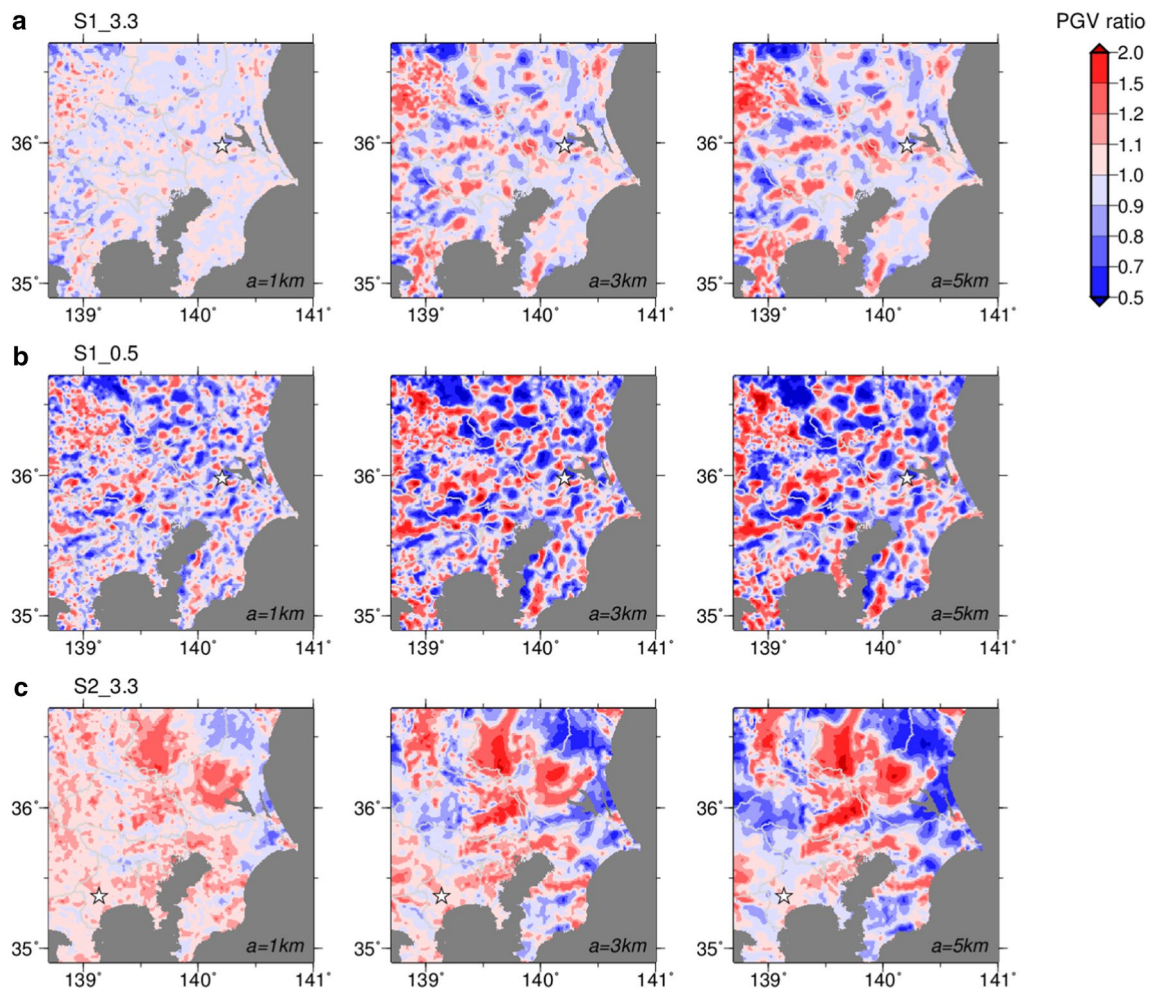


**Fig. 6** Ratio of PGV for homogeneous to heterogeneous velocity models ( $a = 1, 3$ , and  $5$  km) using source models **a** S1\_3.3, **b** S1\_0.5, and **c** S2\_3.3. Epicenters are denoted by stars

where  $Q$  is the quality factor given by  $Q = Q_0 / f_0$  with a reference frequency  $f_0$  (Graves 1996). Here,  $Q_0$  is the frequency-independent quality factor for the  $S$ -wave defined at each grid point, for which we assume the same fluctuation as in  $V_S$  [Eq. (1)] in the upper crust. We use this  $Q$  model for the sake of simplicity in the bandlimited ( $< 1$  Hz) analysis. The reference frequency  $f_0$  is set to 0.33 Hz in this study. Note that waves at frequencies higher than  $f_0$  undergo weaker attenuation compared with those at frequencies lower than  $f_0$ .

## Simulation results

### Ground motion at stations

First, we compare the simulation results obtained from the homogeneous and heterogeneous velocity models at individual stations in terms of velocity waveforms, Fourier amplitude spectra (FAS), and 5% damped velocity response spectra ( $S_v$ ). Figures 3 and 4 show examples of ground motions for the homogeneous and heterogeneous ( $a = 5$  km) velocity models using source models S1\_3.3 and S2\_3.3, respectively. Ratios of heterogeneous to homogeneous models are shown for FAS, which help



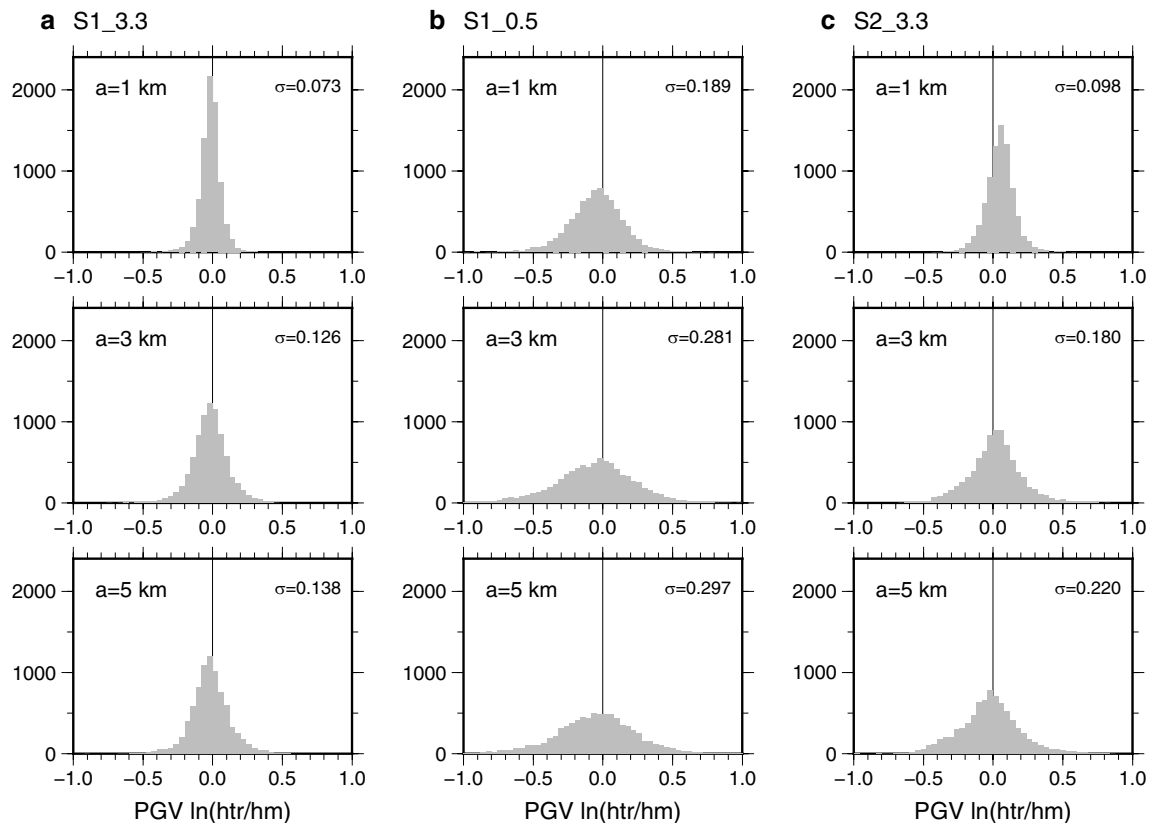


**Fig. 7** Distribution of natural logarithm of heterogeneous-to-homogeneous PGV ratio. Correlation lengths of 1, 3, and 5 km for source models **a** S1\_3.3, **b** S1\_0.5, and **c** S2\_3.3. Standard deviation is indicated on the right top of each panel

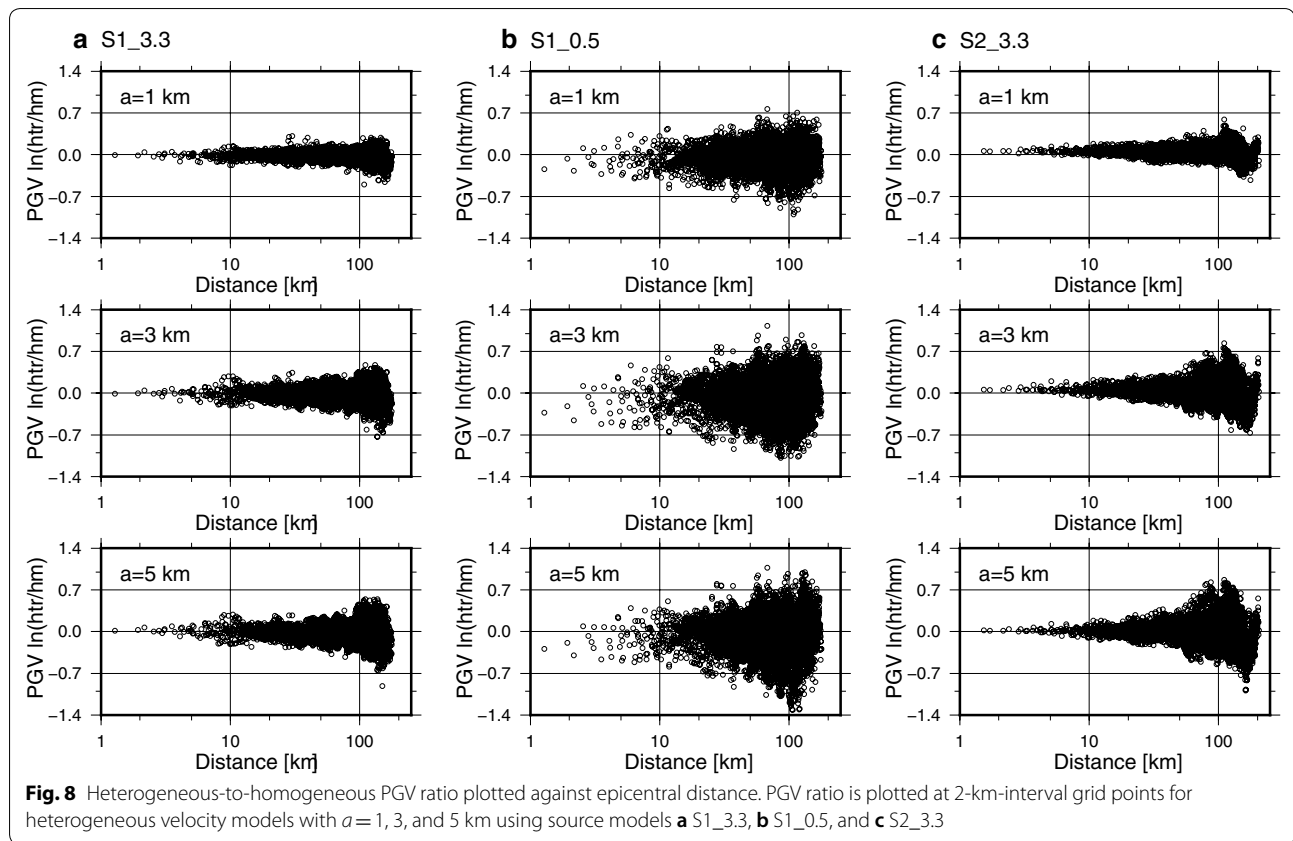
visualizing the effect of introducing crustal heterogeneity in frequency domain. Ground motions for two examples of random heterogeneity with different seeds are plotted by blue and red traces. Station TKY025 is located on the thick sedimentary layers of the Kanto Plain, while GNMH14 is located outside the Kanto Plain (see Fig. 1 for the location of the stations). The depth to the upper crust, where random heterogeneity is applied, is approximately 1500 m and 170 m for TKY025 and GNMH14, respectively, in the velocity model. The epicentral distances for these stations are approximately 90–120 km for both sources S1 and S2.

Changes in the amplitudes and phases of the direct waves and the waves that arrive after the S-wave (early coda) are observed at both stations, indicating interference of the waves caused by scattering and diffraction due to the random heterogeneity in the crust. The amplification of the waveforms of TKY025, located in the

Kanto Plain, is mainly controlled by thick sedimentary layers, especially for the shallower source (S2\_3.3). Still, the effects of the random heterogeneity within the upper crust are observed.

FAS ratios of heterogeneous to homogeneous models, in general, become higher or lower than 1 mainly at frequencies higher than about 0.2 Hz. The effects of heterogeneity in Sv appear in differences in amplitude levels in a frequency range from 0.05 to 1 Hz, as well as in the differences in spectral peaks, as seen in EW component of TKY025 at 0.2–0.5 Hz (Fig. 4).

Velocity waveforms, FAS ratios, and Sv plots at shorter hypocentral distances (approximately 40 km) for S2\_3.3 are shown in Additional file 2, for stations inside and outside the Kanto Plain (KNG001 and TKY001, respectively). Again, we observe that the FAS ratios become noticeably higher or lower than 1 at frequencies higher than about 0.2 Hz for both sites.



The degree of such changes in ground motion due to random heterogeneity depends on the structural properties of the heterogeneity. The maximum amplitudes of the velocity waveforms, for example, can be larger or smaller by a factor of approximately 2, depending on the seed used. It is indicated that the effects of random heterogeneity at individual stations should not be evaluated by a single realization.

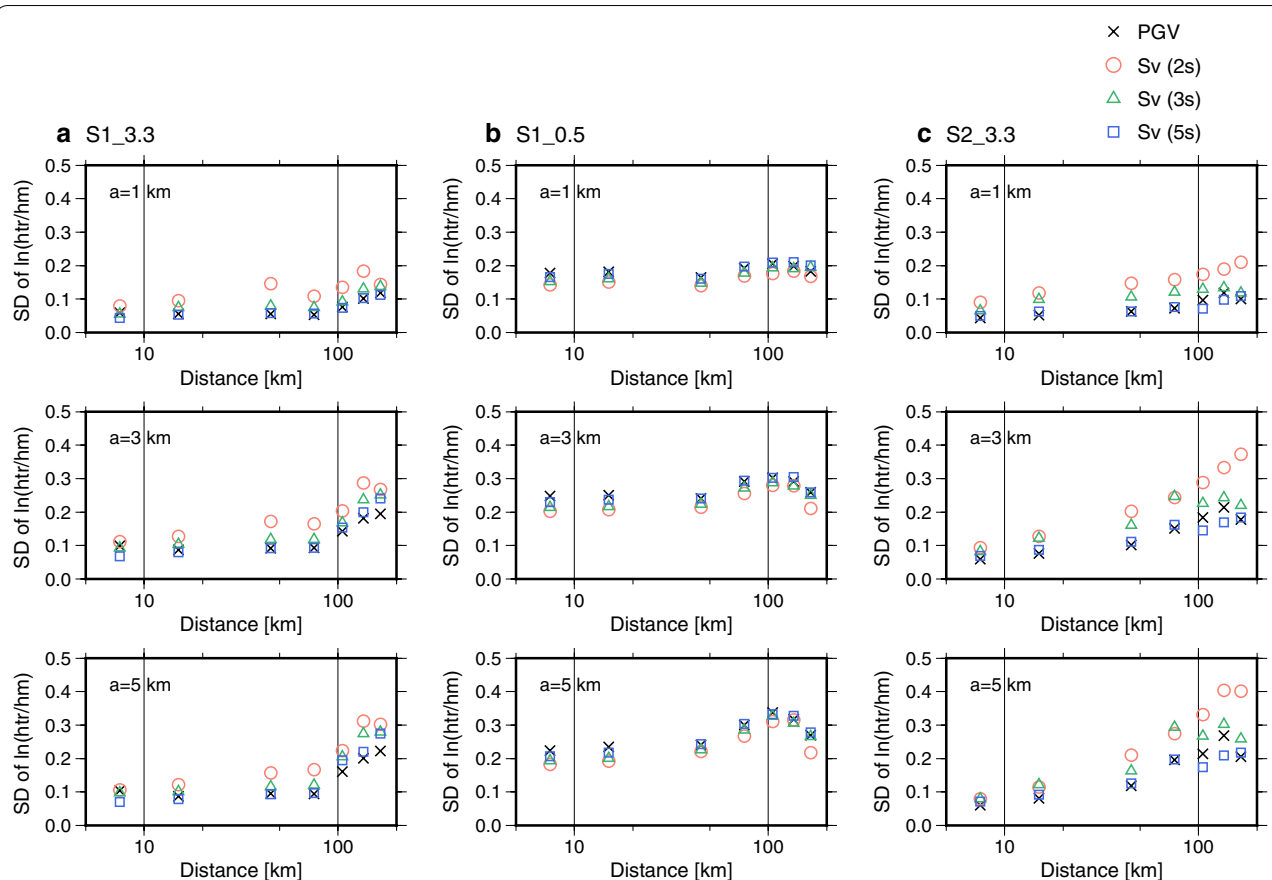
#### Spatial variability of ground motion

Figure 5 shows the distribution of peak ground velocity (PGV) at 2-km-interval mesh for the homogeneous model ( $PGV_{hm}$ ) and the heterogeneous models ( $PGV_{htr}$ ) with  $a = 1, 3$ , and  $5$  km, using the S1\_3.3 source model. Each  $PGV_{htr}$  exhibits overall patterns that are similar to  $PGV_{hm}$ , but with small-scale differences.

In order to clarify the effects of heterogeneity on PGV, the ratio of  $PGV_{htr}$  to  $PGV_{hm}$  (hereinafter PGV ratio) is shown on the map in Fig. 6 for source models S1\_3.3,

S1\_0.5, and S2\_3.3. Note that Fig. 6 shows PGV ratios for a single realization for each case. PGV ratio for four additional realizations for S1\_3.3 with  $a = 5$  km is shown in Additional file 3, which supports the claim that PGV ratio is directly related to the structure of the random heterogeneity, regardless of the location of the source or the sedimentary basin (e.g., Hartzell et al. 2010), because velocity models with different random seeds yield different patterns of PGV ratio.

As shown in Fig. 6, PGV ratio is generally within the range of  $\frac{1}{2}$ –2. In particular, it is from about  $\frac{2}{3}$ – $\frac{3}{2}$  for S1\_3.3. For each source model, PGV ratio is relatively close to 1 for the heterogeneous model with  $a = 1$  km. Small value of  $a$  results in small fluctuations in PGV because it is related to the level of the power spectrum of random heterogeneity at small wave numbers, as Yoshimoto et al. (2015) discussed in their interpretation of the hypocentral distance dependence of amplitude level variance. Comparison of PGV ratio for S1\_3.3 and S1\_0.5



**Fig. 9** Standard deviation of natural logarithm of heterogeneous-to-homogeneous ratio of PGV and Sv (periods 2, 3, and 5 s) plotted against epicentral distance. Standard deviation is computed for distance bins with intervals of 15–30 km. Results for heterogeneous velocity models with  $a = 1, 3$ , and 5 km using source models **a** S1\_3.3, **b** S1\_0.5, and **c** S2\_3.3

indicates that the waves radiated from the shorter-period pulse are more strongly affected by the random structure with relatively long correlation lengths, as compared to waves radiated from the 3.3-s-duration pulse. PGV ratio for S2\_3.3 is larger than that for S1\_3.3, suggesting that the waves radiated from a shallower source travel in the upper crust for a longer distance. Figure 7 shows the distribution of the natural logarithm ( $\ln$ ) of PGV ratio for different correlation lengths, all of which are well described by a normal distribution with a mean of approximately zero.

In Fig. 8,  $\ln$  of PGV ratios at 2-km-interval mesh are plotted with respect to epicentral distance, showing that the variability of PGV ratio generally increases with distance. For S1\_3.3 and S2\_3.3, PGV ratio exceeds a factor of 2 (0.69 in  $\ln$  units) at distances greater than approximately 100 km. PGV ratio for S1\_0.5 is more scattered compared with those for S1\_3.3 and S2\_3.3 and reaches a factor of nearly 4 (1.38 in  $\ln$  units) at approximately 100 km.

In order to clarify the distance dependency, the dataset of PGV ratio is divided into distance bins of 0–15, 15–30, 30–60, 60–90, 90–120, 120–150, and 150–180 km, and the standard deviation (SD) is plotted with respect to distance in Fig. 9. The same analysis is applied to Sv at periods of 2, 3, and 5 s. Since the logarithms of PGV and Sv ratio are the residuals between the homogeneous and heterogeneous models, SD corresponds to within-event ground-motion variability due to the random heterogeneity of the propagation paths. SD generally increases with distance and then reaches a peak at a distance around 100 km. For S1\_3.3 with  $a = 3$  and 5 km, SD for Sv (2 s) reaches 0.3 at a distance of 120–150 km, whereas it is less than 0.2 at distances of less than 90 km. This may be explained by an analogy to amplitude fluctuation of short-period waves in heterogeneous media that saturate at a certain traveling distance (e.g., Hoshiba 2000; Yoshimoto et al. 2015).

In Fig. 10,  $\ln$  of Sv heterogeneous-to-homogeneous ratios averaged over the 174 K-NET and KiK-net

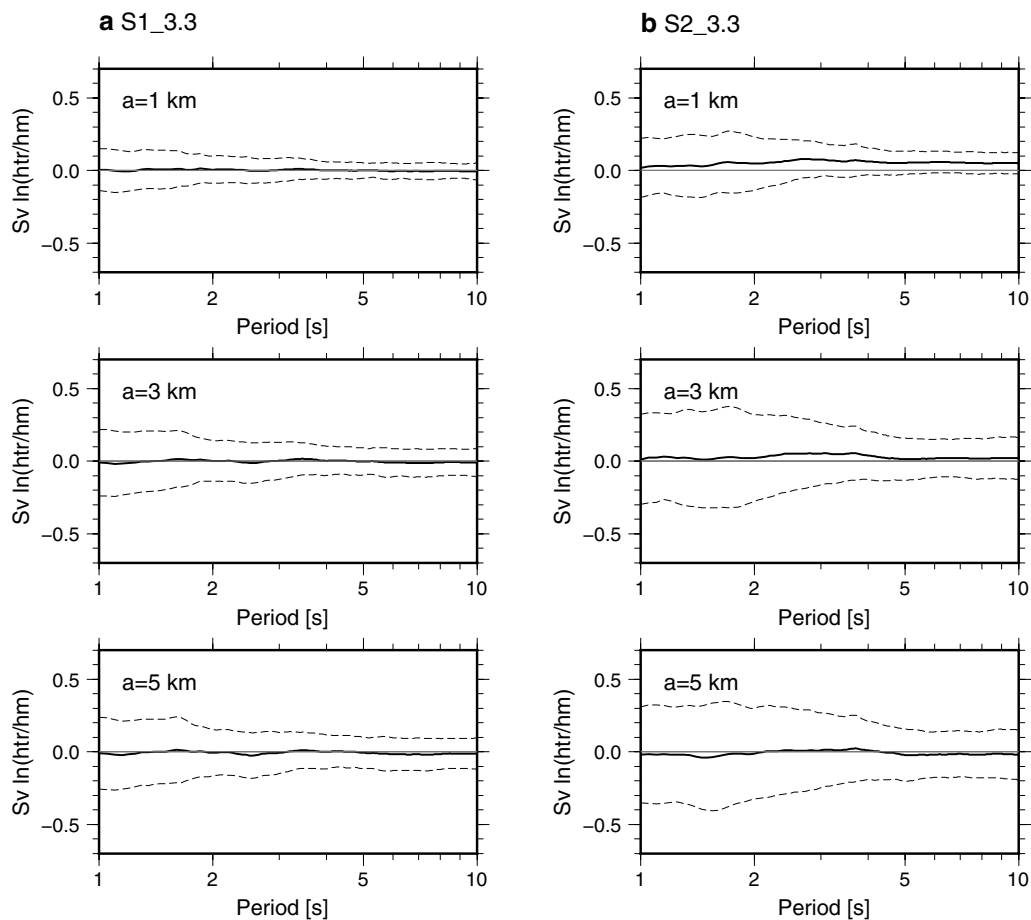


**Fig. 10** Model bias of the heterogeneous model from the homogeneous model for response spectra. Heterogeneous-to-homogeneous ratio of 5% damped velocity response spectra for the heterogeneous velocity models with  $a = 1, 3$ , and  $5$  km is averaged over 172 observation points (K-NET and Kik-net stations; see Fig. 1) and five realizations at each period points, for source models **a** S1\_3.3, **b** S2\_3.3. Standard deviation is plotted by dashed lines

stations (see Fig. 1 for the location) and five realizations of random heterogeneity are plotted for each period, in an attempt to clarify the systematic bias (model bias) of  $S_v$  for the heterogeneous models from that for the homogeneous model. The mean plot is nearly flat at zero at periods from 1 to 10 s for both of the source models S1\_3.3 and S2\_3.3, suggesting that no systematic amplification or deamplification of ground motion was caused by introducing random heterogeneity in the crust in the studied area. On the other hand, SD clearly increases as the period approaches the minimum period of 1 s, up to 0.2–0.3 for the model with  $a = 5$  km.

Our analysis so far used  $\varepsilon = 0.05$  for the standard deviation of the velocity fluctuation. In Fig. 11, we show the effect of the choice of  $\varepsilon$  on PGV ratio and the

model bias of  $S_v$  in the same manner as Figs. 7 and 10, using simulation results for S1\_3.3 with  $a = 5$  km. The standard deviation of the distribution of the PGV ratio increases as the value of  $\varepsilon$  increases; it is 0.10, 0.14, and 0.17 for  $\varepsilon = 0.03, 0.05$ , and  $0.07$ , respectively. The model bias for  $\varepsilon = 0.03, 0.05$ , and  $0.07$  is similar to each other, with the mean plot being flat at zero. SD increases as the period approaches to the minimum period for all cases, but it is smaller for smaller values of  $\varepsilon$ .

## Conclusions

We investigated the effects of short-wavelength heterogeneity in the crust on long-period (periods 1 s and longer) ground motion by conducting 3D finite-difference simulations in the Kanto region of Japan. Heterogeneity in

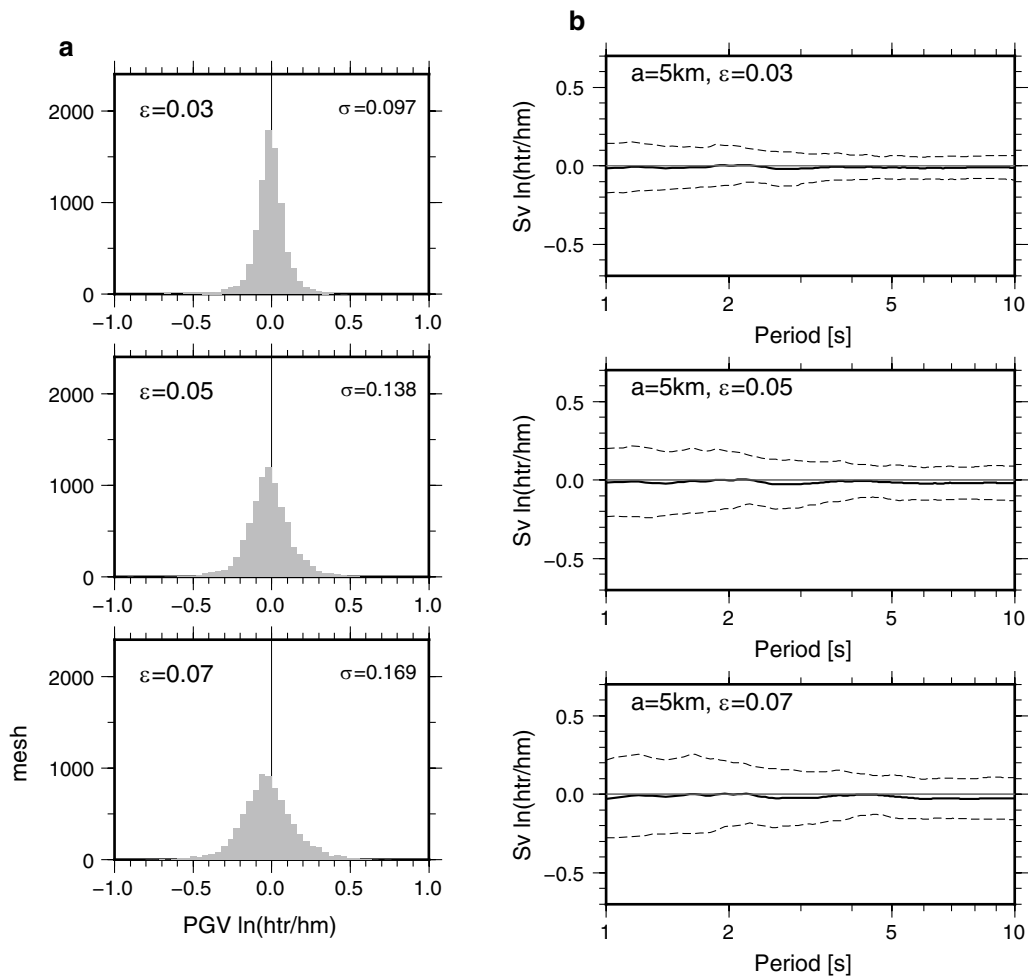


**Fig. 11** Effect of the heterogeneity with different values of standard deviation ( $\varepsilon = 0.03, 0.05$ , and  $0.07$ ). Simulation results for the correlation length of 5 km and the S1\_3.3 source model are used. **a** Distribution of natural logarithm of heterogeneous-to-homogeneous PGV ratio (see Fig. 7 caption for detail). **b** Model bias of the heterogeneous model from the homogeneous model for response spectra with mean (solid lines) and standard deviation (dashed lines). See Fig. 10 caption for detail; note that it is for one random realization

the upper crust ( $V_S = 3200\text{--}3400$  m/s) was modeled by introducing random fluctuations of the seismic velocity characterized by the exponential autocorrelation function. We investigated the effects of the random heterogeneity for PGV, FAS, and Sv on the engineering bedrock ( $V_S \sim 350$  m/s) in terms of mean level and variability, for various correlation lengths, source locations, and source time functions.

Based on numerical simulations, the effects of random heterogeneity on the ground motion appeared in changes in the amplitudes and phases of both the direct waves and later phases, as well as the amplitudes and spectral peaks of FAS and Sv. The degree of such changes differs from place to place and from one realization of random heterogeneity to another.

The distribution of the heterogeneous-to-homogeneous ratio of PGV (PGV ratio) at 2-km-interval mesh was well described by a lognormal distribution with a mean of approximately zero. For a correlation length of 3–5 km and  $\varepsilon = 0.05$ , PGV ratio was found to be within a factor of 2 for a source duration of 3.3 s, whereas it reached a factor of approximately 4 for a source duration of 0.5 s. PGV ratio is significantly smaller for a correlation length of 1 km, suggesting that the correlation length of 1 km is shorter than the dominant wave length in our simulations. PGV ratio for a shallow source at a depth of 8 km (S2\_3.3) is generally larger than that for a deep source at 40 km (S1\_3.3), because the waves radiated from S2 travel in the upper crust for greater distance.



SD of  $\ln$  of PGV ratio generally increases with distance up to a certain value, after which it saturates or decreases. For a correlation length of 3–5 km with a source duration of 3.3 s, SD reaches 0.2–0.3 (in  $\ln$  units; a factor of 1.2–1.3) at distances of approximately 100 km.

We calculated  $\ln$  of Sv ratio averaged over the surface of the computed area and five realizations of random heterogeneity. The mean value is nearly flat at zero for the period range from 1 to 10 s, suggesting that the bias of the heterogeneous model from the homogeneous model is almost negligible in the period range studied herein. The standard deviation increased with decreasing period and was approximately 0.2–0.3 in  $\ln$  units at periods of 1–2 s.

Although the results in this study are derived from simulations with limited combinations of parameters for random heterogeneity, the results provide information to grasp the ground-motion variability due to random heterogeneity in the propagation path for a realistic 3D velocity model in the Kanto region. However, the local characteristics of short-wavelength crustal heterogeneity have not been appropriately modeled at present. A better understanding of crustal heterogeneity, along with source rupture and site responses, is essential to advances in 3D physics-based ground-motion simulations toward frequencies of 1 Hz and higher. As a next step, it is also necessary to include short-wavelength heterogeneity within the sedimentary layers of the Kanto Plain, the characteristics of which differ in scale from those in the crust.

## Additional files

**Additional file 1.** Numerical tests to investigate the effect of heterogeneity in the lower crust. CASE0, CASE1, and CASE2 correspond to the velocity models without random heterogeneity, with random heterogeneity in the upper crust, and with random heterogeneity in the upper and lower crust.

**Table S1.** Description of the point source models. **Figure S1.** Velocity models used in the tests, showing the horizontal plane at depth of zero (top panel), vertical cross-sectional views at  $X=50$  km for CASE1 and CASE 2 (middle and bottom panels, respectively). Triangles and the stars denote the receivers and hypocenter, respectively. Grid spacing for the finite-difference simulations are 100 m and 50 m for the horizontal and vertical directions, respectively, down to the depth of 16 km. **Figure S2.** Velocity waveforms at the receivers for the source at the depth of (a) 10 km and (b) 25 km. Gray, red, and blue lines correspond to CASE0, CASE1, and CASE2. Waveforms are low-pass filtered at 1 Hz.

**Additional file 2: Figure S3.** Additional examples of ground motion at shorter hypocentral distances for S2\_3.3. See Fig. 4 caption for detail.

**Additional file 3: Figure S4.** PGV ratio for four realizations of random heterogeneity that are different from that in Fig. 6. Heterogeneous velocity model with  $a=5$  km and the source model S1\_3.3 are used.

## Abbreviations

3D: three-dimensional; HERP: the Headquarters for Earthquake Research Promotion; JIVSM: Japan Integrated Velocity Structure Model; FAS: Fourier amplitude spectrum; Sv: velocity response spectrum; PGV: peak ground velocity; SD: standard deviation.

## Authors' contributions

AI performed the simulations and data processing and drafted the manuscript. TM and ST helped set up the simulation models and interpret the results. NM and HF contributed to discussion of the results. All authors read and approved the final manuscript.

## Acknowledgements

We thank the editor Takuto Maeda and two anonymous reviewers for thoughtful comments that helped improve this article. Most figures were drawn using the Generic Mapping Tools software (Wessel and Smith 1998).

## Competing interests

The authors declare that they have no competing interests.

## Availability of data and materials

Please contact the corresponding author for data requests. The 3D velocity model of the Kanto region and JIVSM are available from HERP Web site.

## Funding

This study was supported by the "Support Program for Long-period Ground Motion Hazard Maps of Japan" of the Ministry of Education, Culture, Sports, Science, and Technology of Japan.

## Publisher's Note

Springer Nature remains neutral with regard to jurisdictional claims in published maps and institutional affiliations.

Received: 4 July 2018 Accepted: 19 September 2018

Published online: 29 September 2018

## References

- Aoi S, Fujiwara H (1999) 3D finite-difference method using discontinuous grids. *Bull Seism Soc Am* 89:918–930
- Aoi S, Hayakawa T, Fujiwara H (2004) Ground motion simulator: GMS. BUTSURI-TANSA 57:651–666 (in Japanese with English abstract)
- Emoto K, Saito T, Shiomi K (2017) Statistical parameters of random heterogeneity estimated by analyzing coda waves based on finite difference method. *Geophys J Int* 211:1575–1584. <https://doi.org/10.1093/gji/ggx387>
- Frankel A, Clayton RW (1984) A finite-difference simulation of wave propagation in two-dimensional random media. *Bull Seism Soc Am* 74:2167–2186
- Fujiwara H, Kawai S, Aoi S, Morikawa N, Senna S, Kudo N, Ooi M, Hao KXS, Hayakawa Y, Toyama N, Matsuyama H, Iwamoto K, Suzuki H, Liu Y (2009) A study on subsurface structure model for deep sedimentary layers of Japan for strong-motion evaluation. *Tech Note Natl Res Inst Earth Sci Disaster Prev* 337:272 (in Japanese)
- Gaebler PJ, Eulenfeld T, Wegler U (2015) Seismic scattering and absorption parameters in the W-Bohemia/Vogtland region from elastic and acoustic radiative transfer theory. *Geophys J Int* 203:1471–1481. <https://doi.org/10.1093/gji/ggv393>
- Graves R (1996) Simulating seismic wave propagation in 2D elastic media using staggered-grid finite differences. *Bull Seism Soc Am* 86:1091–1106
- Graves R, Pitarka A (2016) Kinematic ground-motion simulations on rough faults including effects of 3D stochastic velocity perturbations. *Bull Seism Soc Am* 106:2136–2153. <https://doi.org/10.1785/0120160088>
- Gusev AA, Abubakirov IR (1999) Vertical profile of effective turbidity reconstructed from broadening of incoherent body-wave pulses—II. Application to Kamchatka data. *Geophys J Int* 136:309–323. <https://doi.org/10.1046/j.1365-246X.1999.00741.x>
- Hartzell S, Harsmen S, Frankel A (2010) Effects of 3D random correlated velocity perturbations on predicted ground motions. *Bull Seism Soc Am* 100:1415–1426. <https://doi.org/10.1785/0120090060>
- Headquarters for Earthquake Research Promotion (2017) National seismic hazard maps for Japan. [https://www.jishin.go.jp/evaluation/seismic\\_hazard\\_map/shm\\_report/shm\\_report\\_2017/](https://www.jishin.go.jp/evaluation/seismic_hazard_map/shm_report/shm_report_2017/). Accessed 18 Sept 2018
- Hisada Y (2001) A theoretical omega-square model considering spatial variation in slip and rupture velocity. Part 2: case for a two-dimensional source

- model. *Bull Seism Soc Am* 91:651–666. <https://doi.org/10.1785/0120000097>
- Hoshiba M (2000) Large fluctuation of wave amplitude reproduced by small fluctuation of velocity structure. *Phys Earth Planet Int* 120:201–217. [https://doi.org/10.1016/S0031-9201\(99\)00165-X](https://doi.org/10.1016/S0031-9201(99)00165-X)
- Imperator W, Mai PM (2013) Broad-band near-field ground motion simulations in 3-dimensional scattering media. *Geophys J Int* 192:725–744. <https://doi.org/10.1093/gji/ggs041>
- Iwaki A, Maeda T, Morikawa N, Aoi S, Fujiwara H (2016) Kinematic source models for long-period ground motion simulations of megathrust earthquakes: validation against ground motion data for the 2003 Tokachi-oki earthquake. *Earth Planets Space* 68:95. <https://doi.org/10.1186/s40623-016-0473-6>
- Koketsu K, Miyake H, Suzuki H (2012) Japan Integrated Velocity Structure Model version 1. In: 15th world conference on earthquake engineering, Lisbon, Portugal, 12–17 Oct
- Magistrale H, Day S, Clayton RW, Graves R (2000) The SCEC Southern California reference three-dimensional seismic velocity model version 2. *Bull Seism Soc Am* 90:565–576
- Okada Y, Kasahara K, Hori S, Obara K, Sekiguchi S, Fujiwara H, Yamamoto A (2004) Recent progress of seismic observation networks in Japan—Hi-net, F-net, K-NET and KiK-net. *Earth Planets Space* 56:xv–xxviii. <https://doi.org/10.1186/BF03353076>
- Sato T, Graves RW, Somerville PG, Kataoka S (1998) Estimates of regional and local strong motions during the great 1923 Kanto, Japan, earthquake ( $M_s$  8.2). Part 2: forward simulation of seismograms using variable-slip rupture models and estimation of near-fault long-period ground motions. *Bull Seism Soc Am* 88:206–227
- Sato H, Fehler M, Maeda T (2012) *Seismic wave propagation and scattering in the heterogeneous earth*, 2nd edn. Springer, Berlin, p 496
- Sekiguchi H, Yoshimi M, Horikawa H, Yoshida K, Kunimatsu S, Satake K (2008) Prediction of ground motion in the Osaka sedimentary basin associated with the hypothetical Nankai earthquake. *J Seismol* 12:185–195. <https://doi.org/10.1007/s10950-007-9077-8>
- Senna S, Maeda T, Inagaki Y, Suzuki H, Matsuyama H, Fujiwara H (2013) Modeling of the subsurface structure from the seismic bedrock to the ground surface for broadband strong motion evaluation. *J Disaster Res* 8(5):889–903. <https://doi.org/10.20965/jdr.2013.p0889>
- Shaw J, Plesch A, Tape C, Suess MP, Jordan T, Ely G, Hauksson E, Tromp J, Tanimoto T, Graves R, Olsen K, Nicholson C, Maechling P, Rivero C, Lovely P, Brankman C, Munster J (2015) Unified structural representation of the southern California crust and upper mantle. *Earth Plan Sci Lett* 415:1–15. <https://doi.org/10.1016/j.epsl.2015.01.016>
- Takemura S, Furumura T, Maeda T (2015) Scattering of high-frequency seismic waves caused by irregular surface topography and small-scale velocity inhomogeneity. *Geophys J Int* 201:459–474. <https://doi.org/10.1093/gji/ggv038>
- Takemura S, Kobayashi M, Yoshimoto K (2017) High-frequency seismic wave propagation within the heterogeneous crust: effects of seismic scattering and intrinsic attenuation on ground motion modeling. *Geophys J Int* 210:1806–1822. <https://doi.org/10.1093/gji/ggx269>
- Wessel P, Smith WHF (1998) New, improved version of generic mapping tools released. *EOS Trans Am Geophys Union* 79:579
- Wirth E, Frankel A, Vidale J (2017) Evaluating a kinematic method for generating broadband ground motions for great subduction zone earthquakes: application to the 2003  $M_w$  8.3 Tokachi-Oki earthquake. *Bull Seism Soc Am* 107:1747–1753. <https://doi.org/10.1785/0120170065>
- Yoshimoto K, Takemura S, Kobayashi M (2015) Application of scattering theory to P-wave amplitude fluctuations in the crust. *Earth Planets Space* 67:199. <https://doi.org/10.1186/s40623-015-0366-0>

**Submit your manuscript to a SpringerOpen<sup>®</sup> journal and benefit from:**

- Convenient online submission
- Rigorous peer review
- Open access: articles freely available online
- High visibility within the field
- Retaining the copyright to your article

---

Submit your next manuscript at ► [springeropen.com](https://www.springeropen.com)